Long-term trend in Black Carbon mass concentration over Central IGP location: Understanding the implied change in radiative forcing

Bharat Ji Mehrotra[1], Atul K Srivastava[2], Amarendra Singh[3], Dirgha Parashar[1], Nabankur M.[1], R. S. Singh[4], Manoj K Srivastava[1†]

[1]Department of Geophysics, Banaras Hindu University, Varanasi, India
[2]Indian Institute of Tropical Meteorology, Ministry of Earth Sciences, New Delhi, India
[3]Centre for Atmospheric Sciences, Indian Institute Technology, New Delhi, India
[4]Department of Chemical Engineering, Indian Institute Technology-BHU, Varanasi, India

†Corresponding author: Manoj K Srivastava (mksriv@gmail.com)

Key Points:

- BC shows significant decreasing trend over central IGP since 2009: maximum in post-monsoon and minimum in pre-monsoon season.
- The BC-ARF also shows decreasing trend over central IGP on yearly scale at the surface, at the top and within the atmosphere since 2009.
- Decreasing trend in BC-ARF within the atmosphere relates to decrease in BC mass concentration and suggests reduced atmospheric warming.

Abstract

Black carbon (BC) has several direct, indirect, semi-direct, and microphysical effects on the Earth's climate system. Analyses of the decade-long measurement of BC aerosols at Varanasi (from 2009 to 2021) was done to understand its impact on radiative balance. General studies suggest that the daily BC mass concentration (mean of 9.18±6.53 μg m^{-3}) ranges from 0.07 to 46.23 μg m^{-3} and show a strong interannual and intra-annual variation over the 13-year study period. Trend analyses suggest that the interannual variability of BC shows significant decreasing trend (-0.47 μg m^{-3} yr^{-1}) over the station. The decreasing trend is maximum during the post-monsoon (-1.86 μg m^{-3} yr^{-1}) and minimum during the pre-monsoon season (-0.31 μg m^{-3} yr^{-1}). The radiative forcing caused specifically by BC (BC-ARF) at the top of the atmosphere (TOA), surface (SUR), and within the atmosphere (ATM) is found to be 10.3 ± 6.4, -30.1 ± 18.9, and 40.5 ± 25.2 Wm^{-2}, respectively. BC-ARF shows strong interannual variability with a decreasing trend at the TOA (–0.47 Wm^{-2} yr^{-1}) and ATM ((–1.94 Wm^{-2} yr^{-1}) forcing, while it showed an increasing trend at the SUR (1.33 Wm^{-2} yr^{-1}). To identify the potential source sectors and the transport pathways of BC aerosols, concentrated weighted trajectories (CWT) and potential source contribution function (PSCF) analyses have been conducted over the station. These analyses revealed that the primary source of pollution at Varanasi originate from the upper IGP, lower IGP, and central India.

Plain Language Summary

Long-term measurement of black carbon (BC) mass concentration was done at a representative Central Indo-Gangetic location, Varanasi, from 2009 to 2021. Analysis suggests significant inte-annual and intra-annual variation of BC mass for the location. Important finding is the significant decreasing trend/year in BC mass: the highest for the post-monsoon season (Oct-Nov) and the lowest for the pre-monsoon (Mar-Apr-May). BC aerosol radiative forcing at the top of the atmosphere, at the surface and within the atmosphere was found to be 10.3 ± 6.4, -30.1 ± 18.9, 40.5 ± 25.2 Wm^{-2}, and forcing within the atmosphere shows a decreasing trend/year. The trend suggests a reduction in the atmospheric heating rate due to black carbon. On the basis of the concentrated weighted trajectories (CWT) and potential source contribution function (PSCF) analyses, the highest contribution is sourced from the upper IGP, followed by lower IGP, and Central India. Except for monsoon season (Jun-Jul-Aug-Sept), the major contributor is the upper IGP, while, during monsoon, the major contributor is the lower IGP, followed by central IGP region.

1 Introduction

Black Carbon (BC) is a prominent absorbing component of carbonaceous aerosols mainly produced due to the incomplete combustion of fossil fuels, biofuels, and biomass burning, etc. (Bond et al., 2013). Despite having a short atmospheric lifetime, it has several direct, indirect, semi-direct, and microphysical effects on Earth's climates (Ackerman et al., 2000; Bond et al., 2013). BC has been reported to have the second-highest global warming potential after CO_2 (Bond et al., 2013; Jacobson, 2001). Due to its strong absorbing nature, it warms the atmosphere and adds to global warming (Bond and Bergstrom, 2006; Haywood and Shine, 1995). BC aerosol impacts the cryosphere (Kang et al., 2020) by depositing on snow surface and hence reducing snow albedo thereby accelerating the snowpack/glaciers melting (Clarke and Noone, 1985; Flanner et al., 2007, 2009; Hansen and Nazarenko, 2004). It also impacts atmospheric dynamics in different ways depending upon the level it is present in the vertical column (Talukdar et al.,

2019). In the higher altitudes, it stabilizes the atmosphere by changing atmospheric temperature profile; whereas in the lower troposphere destabilizes planetary boundary layer, enhancing convective processes and cloud formation (Ding et al., 2016; Li et al., 2017). BC is responsible for the reduction of surface latent heat due to surface cooling and decreasing atmospheric humidity. Differential spatial distribution of BC causes perturbations of regional heating and temperature gradient, which alter the atmospheric circulation and monsoon system (Meehl et al., 2008; Soni et al., 2018). Furthermore, as the time progresses in the atmosphere, BC 'ages', as hydrophobic particles to become hydrophilic and serve as cloud condensation nuclei (CCN) for cloud formation (Conant et al., 2002; Nenes et al., 2002). The cloud droplet formed due to BC particles further heat the cloud droplets and air around it and potentially alter cloud microphysical properties and cloud activation (Conant et al., 2002). Numerous studies have been carried out in recent past due to the unique nature of BC and its impact on the climate system using limited period of data at different locations (Zhu et al., 2021; Dumka et al., 2019; Kalluri et al., 2017; Raju et al., 2015; Singh et al., 2015; Rattigan et al., 2013; Srivastava et al., 2012; Wang et al., 2012.

Understanding the source contribution of BC aerosols is important because they impact air quality, human health, and climate system in several ways. It is furthermore important as they have a widespread global presence. Recently, some studies have highlighted the Indo-Gangatic Planes (IGP) in north India as a hotspot for BC aerosols, and reported BC concentrations as high as 20 - 30 μg m^{-3}, or even higher (Dumka et al., 2018; Singh et al., 2018). Atmospheric BC observations on temporal and spatial scales are, however, sparse across the IGP, that sometimes necessitates the usage of regional and global chemical transport models for BC concentrations estimates (Verma et al., 2022) and associated atmospheric radiative forcing (ARF). The forcing due to BC is highly dependent on its concentration, wind vectors, as well as mixing with other components released in the atmosphere. The Intergovernmental Panel on Climate Change (IPCC) in its Fifth Assessment Report has estimated that the global mean clear-sky radiative forcing due to BC is +0.4 (+0.05 to +0.8) Wm^{-2} (IPCC, 2013).

In view of above, continuous long term BC measurement is done at Varanasi (25.30° N, 83.03° E, 83 m amsl), a representative central IGP location) for a period of 13 years from 2009 to 2021 as part of ISRO's ARFI program. The present study discusses the climatology of BC mass concentration and reports, for the first time, the long-term trend in surface BC mass concentration from any central IGP location. Major source regions and transport pathways of BC were studied on the basis of the potential source contribution function (PSCF) and concentration weight trajectory (CWT) analyses. In addition, BC aerosol optical properties were estimated using the Optical Properties of Aerosols and Clouds (OPAC) model (Hess et al., 1998) and associated radiative forcing were estimated using the Santa Barbara DISORT atmospheric radiative transfer (SBDART) model (Ricchiazzi et al., 1998). The climatic impacts of BC mass concentration on the basis of its radiative characteristics were analyzed and have also been discussed.

2 **Site description and surface meteorology**

Continuous real-time ambient BC mass concentration was measured using a seven-channel aethalometer AE42 (Magee Scientific, USA) from January 2009 to November 2021, at Varanasi. The study area, Varanasi (25.30° N, 83.03° E, ~ 83 m amsl), popularly known as the spiritual capital of India, is in the south-eastern part of Uttar Pradesh state in India. Varanasi is a

representative site in the central IGP. The semi-urban city covers area of around 1535 sq km (Urban 163.78 sq. km.) with a high population density of 2395 resident per square kilometer (Census of India, 2011). Varanasi is among one of the most heavily polluted cities in IGP (Murari et al., 2020; Tiwari et al., 2016a, 2015) and was reported as one of the most toxic cities in the country in the year 2015 (Singh et al., 2021). Large-scale urbanization, small scale industries, extensive commercial activity, heavy vehicular emission due to congestion, road resuspended dusts, agricultural burning activities, emission from domestic cooking in outskirts of the city, and wood/ waste burning are the major local aerosol source (Singh et al., 2015).

The study site has a humid subtropical climate which is often influenced by a wide range of synoptic weather events, with ocean and Himalayan influences being the modest (Kumar et al., 2017). The region experiences strong seasonal patterns with four seasons: cold and chilly winter (December to February), hot and dry summer or Pre-Monsoon (March to May), strong rainfall during monsoon (June to September), and the post-monsoon season (October and November).

The monitoring location experiences westerly wind during summer and winter while easterly wind during monsoon (Murari et al., 2016). Averaged monthly variation in weather parameter (temperature, relative humidity, rainfall including atmospheric boundary layer altitude) over the study site is shown in the figure 1, and their annual variations are shown in figure 1. The data for the weather parameters was obtained from the co-located India Meteorological Department station. The atmospheric boundary layer altitude data was obtained from MERRA-2 data (M2TMNXFLX). The variability in the weather parameters shown in the figure 1 are based on the daily observation averaged on the monthly scale. From thirteen years of observations (2009-2021), weather parameters over Varanasi shows sharp temporal pattern. The maximum values of surface temperature were observed in the month of June (34.1 ± 3.2 °C) and minimum were observed in January (15.9 ± 2.8 °C), whereas annual variation in surface temperature is very much consistent over the years (Figure 1-e). Maximum annual average temperature was observed in 2009 (28.2 ± 6.2 °C) and minimum was observed in 2011 (25.2 ± 6.6 °C). Relative humidity (RH) varies opposite to the temperature with minimum values in April (40.7 ± 13.3 %) and maximum during the August months (83.5 ± 7.5 %). Notably, April month is a representative summer month, and August is a representative monsoon month for the regions. Region received annual average rainfall of 925±241 mm during the study period out of which around 85% of its total annual rainfall received during the monsoon months (June to September). Over the years, the rainfall is showing the increasing trend with an increase of 38.7 mm yr^{-1}. During the winter months, winds move eastward due to the presence of extratropical low-pressure system (called westerly disturbances), and it brings occasional rain or frequent fog in the region.

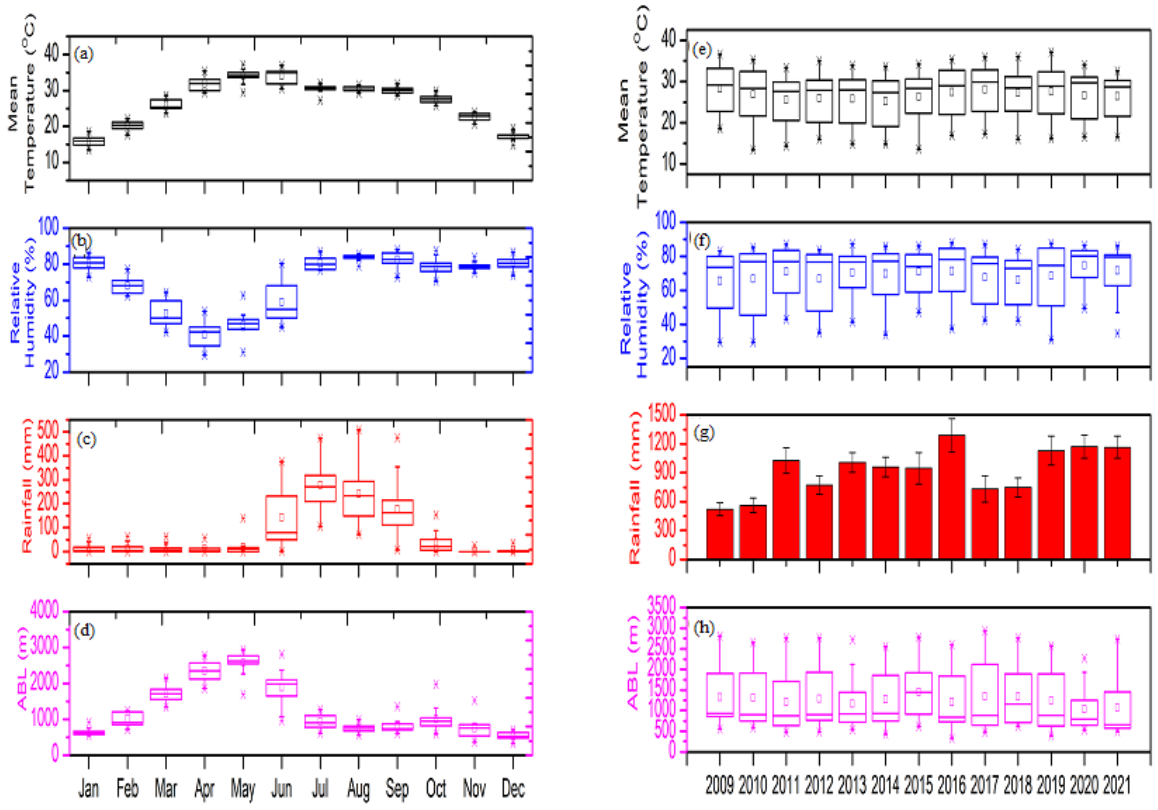

Figure 1. Monthly variability of weather parameters observed over Varanasi (a) Mean Temperature (b) Relative Humidity (c) Rainfall and (d) atmospheric boundary layer (ABL) height during 2009-2021 and Interannual variability of weather parameters observed over Varanasi (e) Mean Temperature (f) Relative Humidity (g) Rainfall and (h) atmospheric boundary layer (ABL) height during 2009-2021.

3. Instrumentation and Methodology

3.1. Measurements of BC aerosols and Data analysis

Continuous and regular real-time ambient BC mass concentration was measured using seven-channel (370, 470, 520, 590, 660, 880, and 950 nm) Aethalometer AE42 (Magee Scientific, USA). The instrument was kept at an altitude of 15m from the ground, away from any direct source of BC, and operated at a sampling interval of 5 min with standard flow rate of 5.0 L/min. The aethalometer was properly calibrated for the flow rate on regular basis. The aethalometer works on the principle of the attenuation of light (ATN) transmitted through the aerosols deposited on filter tape at seven different wavelengths. The ATN is directly proportional to the amount of BC mass loading on the filter tape (Hansen et al., 1984).

$$b_{ATN} = \frac{A}{V}\frac{\Delta ATN}{\Delta t} \quad (1)$$

Where b_{ATN} is the light attenuation coefficient, ΔATN is the change in attenuation during the time period 't', A is the aerosol spot area, and V is the air-flow rate shown in equation (1). The

value of attenuation corresponding to 880nm was considered for the calculation of BC mass using a mass absorption cross section (MAC) of 16.6 m^2 g^{-1}, provided by the manufacturer.

$$BC = \frac{b_{ATN}}{MAC} \quad (2)$$

Multiple light scattering inside the filter matrix causes increased absorption, resulting in aethalometer measurements errors. Ideally, light attenuation should increase linearly with BC loading on filter paper. However, when the BC mass on the filter increases, the linearity between attenuation and BC loadings decreases owing to 'loading effects,' resulting in underestimation of BC mass concentration (Virkkula et al., 2007; Weingartner et al., 2003). To obtain spectral absorption coefficient (b_{abs}), the corrections for the multiple light scattering in filter tape and loading effect were done using the methodology used by Dumka et al., (2019) and reference therein in their study.

$$b_{abs} = \frac{b_{ATN}}{CR(ATN)} \quad (3)$$

Here, C is the multiple light scattering inside the filter matrix and R(ATN) is the loading correction due to BC builds on the filter tape over time shown in equation (3).

3.2. Trend analysis of BC

Several studies have used non-parametric statistical analysis, such as Mann-Kendall (MK) test, to estimate multi-year trends globally (Kumar et al., 2021; Collaud Coen et al., 2020; Mohammad et al., 2022; Zhao et al., 2017). Due to the common issue of serial correlation for time series data with the MK test, the modified Mann-Kendal test proposed by Yue and Wang (2004) was used in the study. The detailed descriptions of MK and modified MK test are given elsewhere (Kendall, 1957; Mann, 1945; Yue and Wang, 2004).

3.3. Potential Source Contribution Function and Concentration-Weighted Trajectory

The air mass backward trajectories obtained from the Hybrid Single Particle Lagrangian Trajectory (HYSPLIT) model (Stein et al., 2015) were used to analyze the potential source sectors and transport pathway of measured black carbon at Varanasi. The Potential Source Contribution Function (PSCF) and Concentration-Weighted Trajectory (CWT) analyses were performed with 5-day backward air mass trajectories using MeteoInfo software(Wang, 2019, 2014). Five days back air mass trajectory was calculated for every 24hours at the 500m height above the ground level using NCEP reanalysis data during the study period from January 2009 to December 2021. The PSCF is wieldy used for the estimation of the probability map of the source of air pollutants (Singh et al., 2021, 2022; Huang et al., 2012; Kant et al., 2020; Sen et al., 2017; Singh et al., 2018). It combines measured pollutants mass concentration with air mass back trajectory for the analysis. CWT analysis was used to determine the source strength of the grid cell to the receptor site based on the weighted concentrations of the trajectories. The PSCF and CWT is defined by Wang et al., (2009) as;

$$PSCF_{ij} = \frac{n_{ij}}{N_{ij}} \quad (4)$$

$$CWT_{ij} = \frac{\sum_{k=1}^{N} C_k T_{ijk}}{\sum_{k=1}^{N} T_{ijk}} \quad (5)$$

In PSCF, n_{ij} represents the frequency of trajectory passages through the specific cell (i,j), while N_{ij} denotes the number of trajectory points in the cell (i,j), corresponding to trajectories with pollutant concentrations higher than a threshold value (Wang et al., 2009). In CWT, the weighted concentration of BC in trajectory in the cell (i,j), k and N denote the trajectory indices and total number of trajectories, respectively. C_k is the concentration of BC observed at receptor site on arrival of trajectory k and T_{ijk} is the residential time of trajectory k in the cell (i,j).

3.4. Estimations of optical and radiative properties of BC

Different aerosol optical properties i.e., aerosol optical depth (AOD), single scattering albedo (SSA), and asymmetry parameter (AP) are required to perform the radiative forcing calculation. Direct measurement of Black Carbon optical properties was not available, so Black Carbon optical properties were estimated by using the Optical Properties of Aerosols and Clouds (OPAC) model (Hess et al., 1998) following Tiwari et al. (2016a, 2016b) and Verma et al. (2013). In this model, optical characteristics of atmospheric aerosol and cloud may be determined for 61 spectral bands between 0.25 and 40 μm. The OPAC model is frequently used and well-accepted method to get the required optical properties. It uses Mie Scattering theory for estimating the aerosol optical characteristics for aerosol mixtures. Further details about the OPAC model are given elsewhere (Hess et al., 1998; Koepke et al., 2015; Singh et al., 2014; Srivastava et al., 2020; Tiwari et al., 2016a).

The model-derived BC optical properties from OPAC, observed column ozone (obtained from co-located Ozone Unit of India Meteorological Department), columnar water vapor (MODIS- Aqua), and surface albedo (Aura OMI version 3) data are used as input in Santa Barbara DISORT atmospheric radiative transfer (SBDART) model (Ricchiazzi et al., 1998) to compute shortwave (0.30–3.0 μm) direct BC aerosol radiative forcing (DARFBC) separately for the top of atmosphere (TOA) and surface at each 1-hr time interval, with and without BC aerosols. In the present study, standard tropical atmospheric profiles of pressure, temperature, and relative humidity (RH) were used as input to the SBDART model, following the methods suggested by previous studies (Kedia et al., 2010; Srivastava et al., 2020). The diurnally averaged direct aerosol radiative forcing (DARF) at the TOA and surface is then used for the net flux calculation according to the following equation (6)

$$DARF_{\text{TOA,SUR}} = (F^{\downarrow}_{with} - F^{\uparrow}_{with})_{\text{TOA,SUR}} - (F^{\downarrow}_{w/o} - F^{\uparrow}_{w/o})_{\text{TOA,SUR}} \quad (6)$$

Where arrows indicate upward (↑) and downward (↓) direction of the radiation fluxes, Fwith and Fw/o indicate the radiation fluxes ‘with’ and ‘without’ aerosol, respectively. Further, the DARF within the atmosphere ($DARF_{ATM}$) was calculated by subtracting the $DARF_{surface}$ from the $DARF_{TOA}$, as shown in equation (7). This is considered as the amount of energy trapped by aerosol in the atmosphere.

$$DARF_{\mathrm{ATM}} = DARF_{\mathrm{TOA},} - DARF_{,\mathrm{SUR}} \quad (7)$$

The atmospheric heating rate which expresses the heating or cooling effect due to aerosol is computed from the first law of thermodynamics, considering the hydrostatic equilibrium of the atmosphere, as following,

$$\frac{\partial T}{\partial t} = \frac{g}{C_p} * \frac{DARF_{\mathrm{ATM}}}{\Delta P} * 24(hr\ /\ day) \times 3600(sec\ /\ hr) \quad (8)$$

where $\partial T/\partial t$ is the heating rate in Kelvin per day (K day^{-1}), g/C_p is the lapse rate, g is the acceleration due to gravity, Cp is the specific heat capacity of air at constant pressure (i.e. 1006 Jkg^{-1}K^{-1}), and ΔP is the atmospheric pressure difference (taken ΔP as 300 hPa).

4 Results and Discussion

4.1 Time series and trend analysis of BC from 2009 to 2021

The primary goal of this work is to understand the long-term trend in surface BC and its potential impacts on our climate system through radiative forcing over the study region. The average black carbon concentration during the study was 9.25 ± 7.66 µg m^{-3}, while, daily mean BC mass concentration varied from 0.07 to 46.23 µg m^{-3}. Minimum BC concentration were observed during the COVID19 lockdown condition whereas the highest were observed during the 2012 winters. Singh et al. (2015, 2018) reported high values of BC during winter 2012 (6.3± 2.7 µg m^{-3}). and winter 2013 (6.5 ± 3.8 µg m^{-3}) for a not far location, Dhanbad city. Dumka et al., (2013) reported 4.45 µg m^{-3} for Hyderabad during 2009-2010, and Sandeep et al., (2013) reported 4.0 µg m^{-3} for Mumbai during 2009-2010. Tiwari et al., (2009) reported an annual mean of 14 ± 12 µg m^{-3} for BC over New Delhi during 2007. The values at Varanasi were greater than many cities in country but less than the BC mass concentration reported over New Delhi. The box plot in Figure 2 shows the statistical details of the yearly variations of BC mass concentration over Varanasi from 2009 to 2021 obtained from daily mean BC mass concentration data.

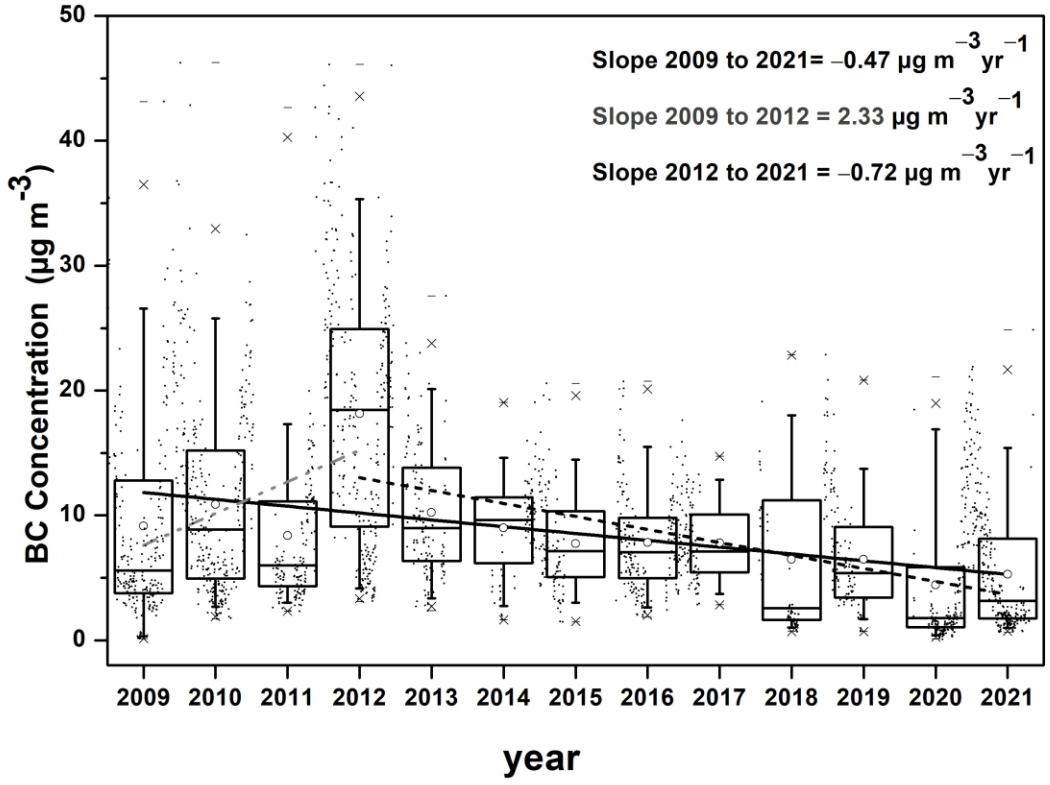

Figure 2. Yearly variability of BC Concentration (µg/m3) at Varanasi during 2009 - 2021.

Boxes in the box plot represent the 25th and 75th percentiles limits, respectively. Lower and upper whiskers represent the 5th and 95th percentiles, and lower and upper crosses represent the 1st and 99th percentiles, respectively. Maximum and minimum values are presented by a dash. The horizontal bar inside represents the median (50th percentile), the open circle represents the mean values. Figure suggest a decreasing trend of BC mass at –0.47 μg m^{-3} yr^{-1} over Varanasi during 2009 to 2021 (figure 2) shown with dark black line. This decreasing trend was, however, initially increasing for the period 2009 to 2012 (+2.33 μg m^{-3} yr^{-1}), that later shows a decreasing trend from 2012 till 2021 (–0.72 μg m^{-3} yr^{-1}). A salient decreasing trend is over the peninsular India also (Manoj et al., 2019). BC shows strong diurnal variation throughout the 13-year study period across all the month/seasons, with a typical bimodal pattern having two isolated packs during the morning and evening hour, and a dip in the concentration of BC during noon hours, as shown in figure 3 and figure 4.

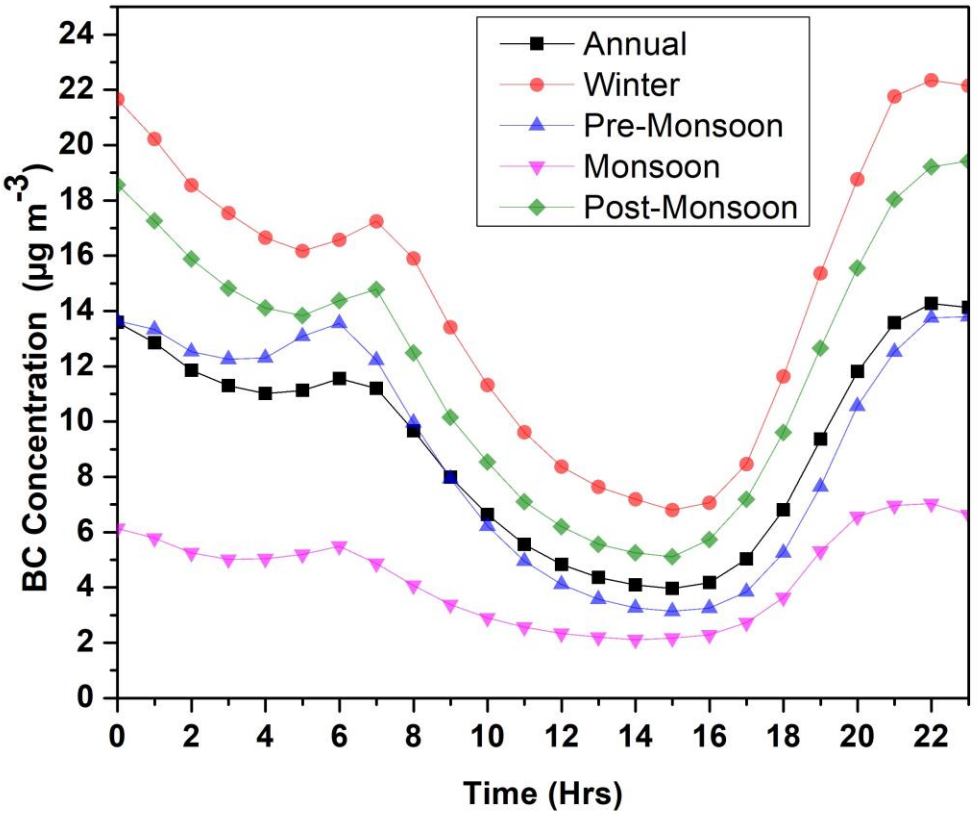

Figure 3. Annual and sessional diurnal variation of BC mass concentration during 2009 to 2021.

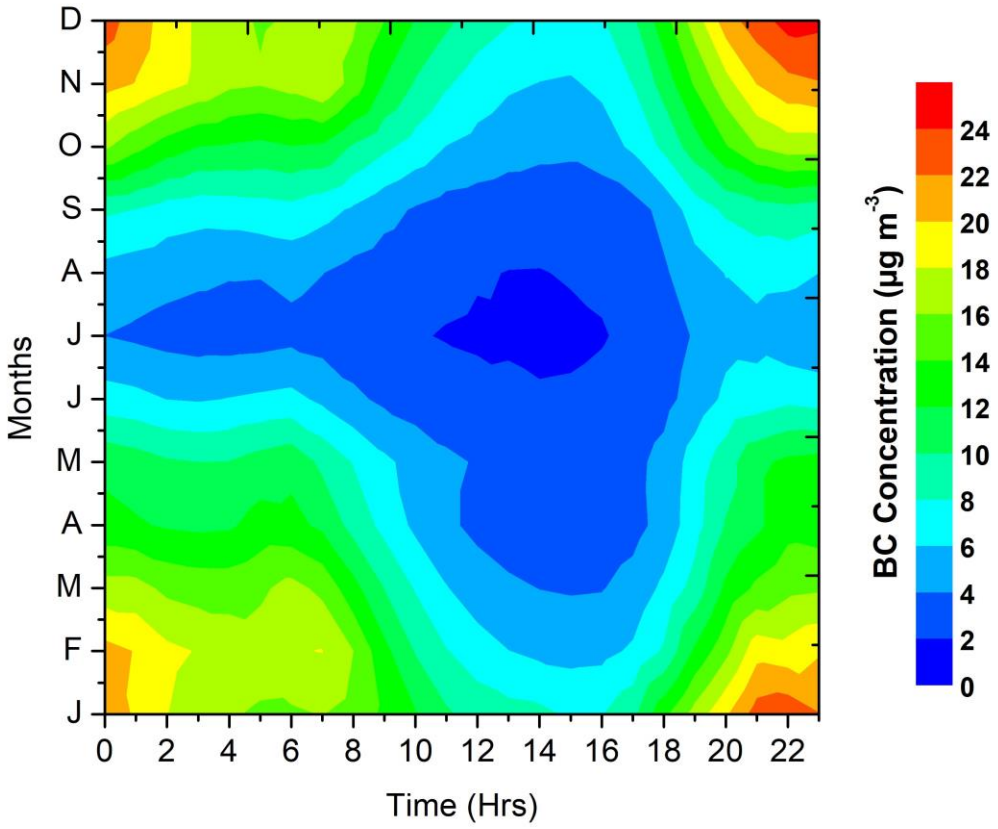

Figure 4. Monthly diurnal variation of BC Concentration (µg/m3) at Varanasi during 2009 - 2021.

Maximum concentration is observed during the winter months, followed by post-monsoon, pre-monsoon and monsoon season. During the winter and post-monsoon seasons, the morning peak was found to be at 07:00 hr local time, whereas during the pre-monsoon and monsoon seasons, the morning peak shifted by an hour to be at 08:00 hr. The evening peak was found at around 22:00 hr during all the seasons. In the monthly color contour diurnal behavior (Figure 4) monsoon months was found to witness maximum dip during noon hours compared to any other season. The seasonal variation of the BC mass concentration is shown in Figure 5 as a box plot, where the statistics shown are arrived at by considering the data from corresponding days falling in the particular seasons: DJF: winter; MAM: pre-monsoon; JJAS: monsoon; and ON: post-monsoon.

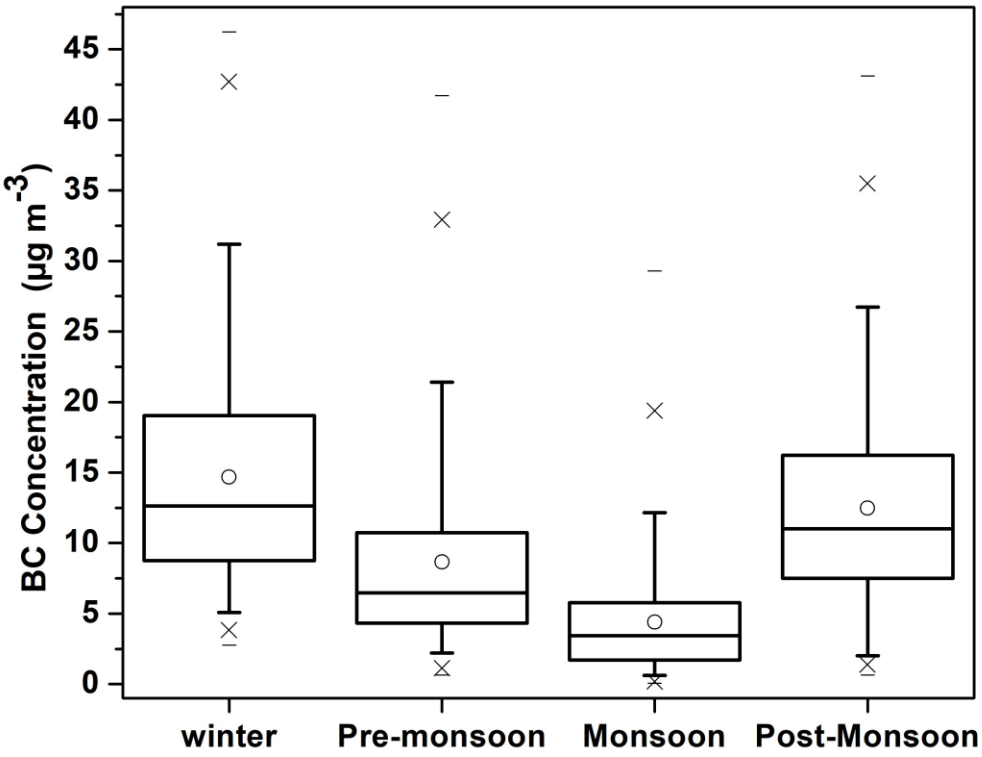

Figure 5. Statistics shown are achieved by considering the data from corresponding days falling in the various seasons. Boxes in the box plot shown here represents the 25th and 75th percentile, respectively. Lower and upper whiskers represent the 5th and 95th percentile, and lower and upper cross represent 1st and 99th percentile, respectively. Maximum and minimum is represented by dash. While the horizontal bar inside represents the median (50th percentile) and open square represent the mean values

Table 1. Monthly, seasonal and annual means of BC mass concentration (BC), BC aerosol optical depth at 500nm (BC-AOD500), BC aerosol radiative forcing at top of the atmosphere (BC-ARF-TOA), at the surface (BC-ARF-SUR) and within the atmosphere (BC-ARF-ATM).

Month	BC ($\mu g/m^3$)	BC-AOD500	BC-ARF-TOA (W/m^2)	BC-ARF-SUR (W/m^2)	BC-ARF-ATM (W/m^2)
Jan	15.0±12.9	0.122±0.063	7.34±2.93	-26.19±11.29	33.53±14.23
Feb	13.3±10.9	0.152±0.044	10.44±2.36	-34.98±8.58	45.42±10.94
Mar	10.7±10.3	0.189±0.082	13.99±4.49	-45.71±16.3	59.71±20.79
Apr	8.2±8.6	0.193±0.098	17.07±6.2	-47.6±19.72	64.68±25.91
May	7.6±10	0.184±0.164	17.31±10.43	-43.98±30.95	61.29±41.35
Jun	4.7±6.4	0.099±0.076	11.21±6.73	-26.16±17.22	37.37±23.95
Jul	3.1±3.9	0.052±0.022	5.77±2.23	-14.39±5.72	20.16±7.96
Aug	4.0±4.0	0.051±0.02	5.01±1.85	-13.88±5.24	18.89±7.08
Sep	5.8±6.2	0.067±0.032	6.08±2.74	-17.38±8.05	23.46±10.79
Oct	10.3±9.2	0.122±0.084	9.29±5.28	-28.28±17.28	37.56±22.55
Nov	13.8±10.9	0.136±0.066	9.24±3.67	-29.43±12.43	38.67±16.10
Dec	15.5±10.6	0.109±0.046	7.69±3.64	-25.41±12.53	33.1±16.16
Winters	15.3±5.9	0.135±0.05	8.8±2.7	-30.1±9.9	38.9±12.5
Pre-Monsoon	8.1±5	0.178±0.102	15.4±6.3	-43.7±19.9	59±26.2
Monsoon	4.1±2.4	0.068±0.031	7.3±2.8	-18.2±7.5	25.4±10.3
Post-Monsoon	12.9±5.5	0.129±0.069	9.3±4.1	-28.9±13.7	38.1±17.9
Annual	9.3±6.6	0.126±0.09	10.3±6.4	-30.1±18.9	40.5±25.2

Overall, seasonal mean BC concentration during the study period (Fig. 6), showed a high value during the winter season (14.67 ± 5.33 μg m^{-3}), followed by the post-monsoon season (12.60 ± 4.87 μg m^{-3}), pre-monsoon season (9.01 ± 4.18 μg m^{-3}) and the monsoon season (4.40 ± 1.70 μg m^{-3}). On the monthly scale (Table 1), maximum average monthly values belong to December (15.5±10.6 μg m^{-3}) and minimum, to the July month (3.1±3.9 μg m^{-3}). The increased use of biomass for heating during winter nights in the surrounding area, the use of fossil fuel, and the unfavorable meteorological conditions for dispersion favors not only BC but also the other aerosol concentrations high during the winter and post-monsoon periods (Kanawade et al., 2020; Kumar et al., 2017; Rajput et al., 2013). On a regular basis, during the post-monsoon season, the main contribution to BC comes from paddy residual burning mostly from the northwest part of India, and during the pre-monsoon season, BC comes from wheat residue burning over the IGP region and Pakistan (Latha et al., 2017; Rajput et al., 2014).

The modified Mann-Kendal test has been applied for all the seasons and results are shown in Figure 6. A decreasing trend in BC mass concentration was observed over the study region, with the highest rate of decrease in post-monsoon (–1.86 μg m^{-3} yr^{-1}) and the least decrease during the pre-monsoon season (–0.31 μg m^{-3} yr^{-1}). In another study over Varanasi, Singh et al., (2015) described the variability of BC mass concentration and its impact on

columnar aerosol optical properties, and crucial surface meteorology and found major sources of BC were form fossil fuel for the year 2009.

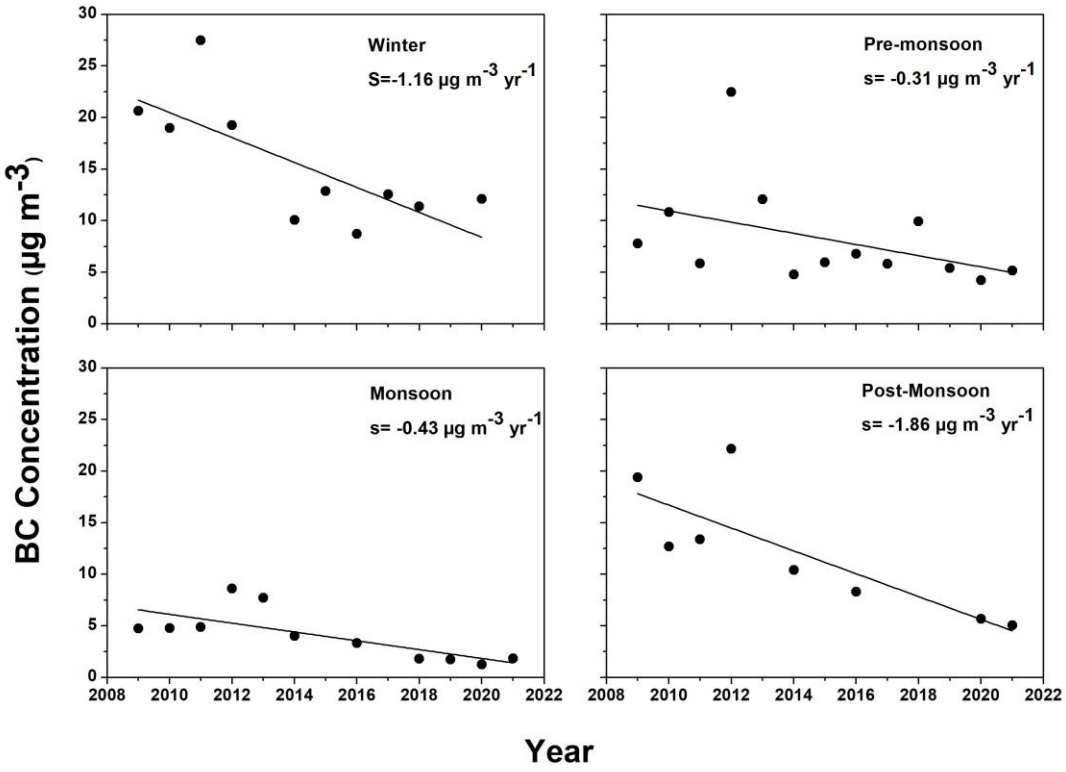

Figure 6. Trend of BC mass Concentration (µg/m3) at Varanasi between 2009 and 2021.

4.2 Source identification of BC mass concentration in different Seasons

An attempt has been made to understand the possible emission sources and the transport pathways of BC aerosols over the study station using potential source contribution function (PSCF) and concentration weight trajectory (CWT) analyses, using the backward air mass trajectories as obtained from HySPLIT model. Figure 7 shows the Potential Source Contribution Function (PSCF) maps during each season for 2009 to 2021. The maps indicate the probabilities of the potential source areas that could be contributing to enhance the BC mass at the study location. PSCF maps are plotted using color codes from light yellow to dark brown, grids having light yellow and yellow shades (PSCF<~0.2 – 0.3) indicates the presence of weak or insignificant sources at the receptor site, grids having yellowish and light brown shades (PSCF<~0.4 – 0.5) indicates probability of presence moderate probability of sources in those cells, whereas cells with brown to dark brown shades (PSCF>~0.7 -0.8) indicates higher probability of potential sources of BC mass concentration at the Varanasi.

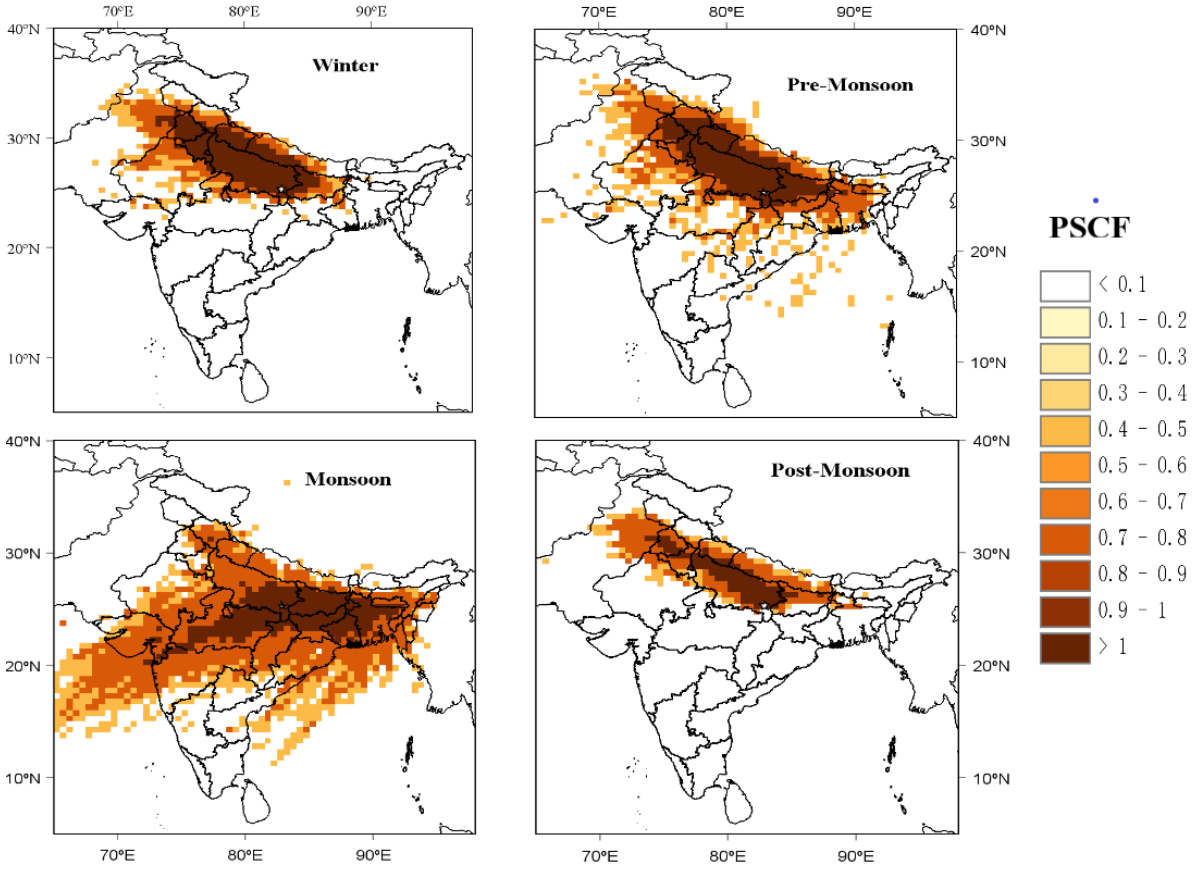

Figure 7. Weighted Potential Source Contribution Function (PSCF) maps of BC over Varanasi during 2009 to 2021.

The transported pollutants play important roles in the BC concentration at the Varanasi throughout the study period. During pre-monsoon and post -monsoon periods winds coming from north, northwest and northeast carry particulates and BC in abundance. Potential reason for

the abundance of pollution is agricultural burning and forest fires (Latha et al., 2017). Many studies done over the IGP region indicates existence of natural and man-made sources of aerosols throughout the region (Lodhi et al., 2013; Srivastava et al., 2020; Tiwari et al., 2009).

PSCF analysis shows the potential source sector, that can be categorized as the BC reception from the upper IGP, Bay of Bengal, Arabian Sea, central highlands, southern peninsular region, Pakistan, and even the Central East Asia region. During the winter months, when the atmosphere is relatively stable compared to other seasons, most of the long-range BC reaches to the site from the upper IGP (Punjab, Haryana, New Delhi, and Rajasthan) and further west. During pre-monsoon or summer period, long range BC sources do not show any regular pattern, rather show potential sources are from multiple source regions, including the upper IGP, the western dry region of India, the semi-arid region of Pakistan and also from the lower IGP region situated in the east of the Varanasi (Bihar, West Bengal, and Jharkhand), as well as from Bangladesh, and the Bay of Bengal region. During the monsoon months, potential source regions are from oceanic region (from the Bay of Bengal and the Arabian Sea), central India, the Deccan Plateau, and the southern Indian region. In the monsoon season, winds are relatively low in aerosols loading as compared to winds coming to Varanasi during other seasons. During this season, the entire north India experiences rain, which leads to wet scavenging of the particles to ultimately show low mass concentrations. During the post-monsoon months, however, the potential sources of BC aerosols are form the upper IGP region (Punjab, Haryana and Western Uttar Pradesh).

To further understand the source CWT analyses of BC mass concentration for Varanasi during each season during 2009 to 2021 was done and shown in Figure 8. These maps indicate spatial distribution of the weighted trajectory concentrations around the receptor site and help to understand the relative contribution of potential source of BC mass concentration. CWT maps are plotted using color scale from blue to pink. For the winter months, grids having green and blue shades indicates the presence of weak sources (CWT<10) and represent a lower probability of potential sources in those cells, whereas cells with yellowish and reddish shades indicate the presence of strong BC mass sources (CWT>10). During the winter months, the BC reaches the receptor site from the upper IGP region with the dominance of source and high CWT values for,Western Uttar Pradesh, Punjab, Haryana, eastern Rajasthan, and regions in the west, including Pakistan. During Pre-monsoon or summer months, grids having violet and blue shades indicate the presence of weak sources (CWT<6) and represent a lower probability of potential sources in those cells, whereas cells with greenish and yellowish shades indicates the presence of strong BC mass sources (CWT>6). Strong sources are from the upper IGP, the dry region of western India, the semi-arid region of Pakistan and weak sources are from the lower IGP region situated in the east of the Varanasi (Bihar, West Bengal, and Jharkhand), Bangladesh, and the Bay of Bengal region. During the monsoon months, the grids having violet and blue shades indicates the presence of weak sources (CWT<4) and represent a lower probability of potential sources in those cells, whereas cells with greenish shades indicates the presence of strong BC mass sources (CWT>4). Overall, during the winter months, long range sources are weak due to wet deposition of BC aerosol due to winter rains, associated with western disturbances. Throughout the monsoon months, winds are coming from the oceanic region (from the Bay of Bengal and the Arabian Sea), central India, the Deccan Plateau, and the southern Indian region, but carry relatively low BC aerosols but the local sources are strong in these months. During the post-monsoon months, the grids having green and blue shades indicates the presence of weak

sources (CWT<10) and represent a lower probability of potential sources in those cells, whereas cells with yellowish and reddish shades indicates the presence of strong BC mass sources (CWT>10). BC reaches the receptor site from the upper IGP region with the dominance of source and high CWT values for the Punjab, Haryana, Western Uttar Pradesh and local sources. CWT map for the post-monsoon also depicts presence of sources from Pakistan region.

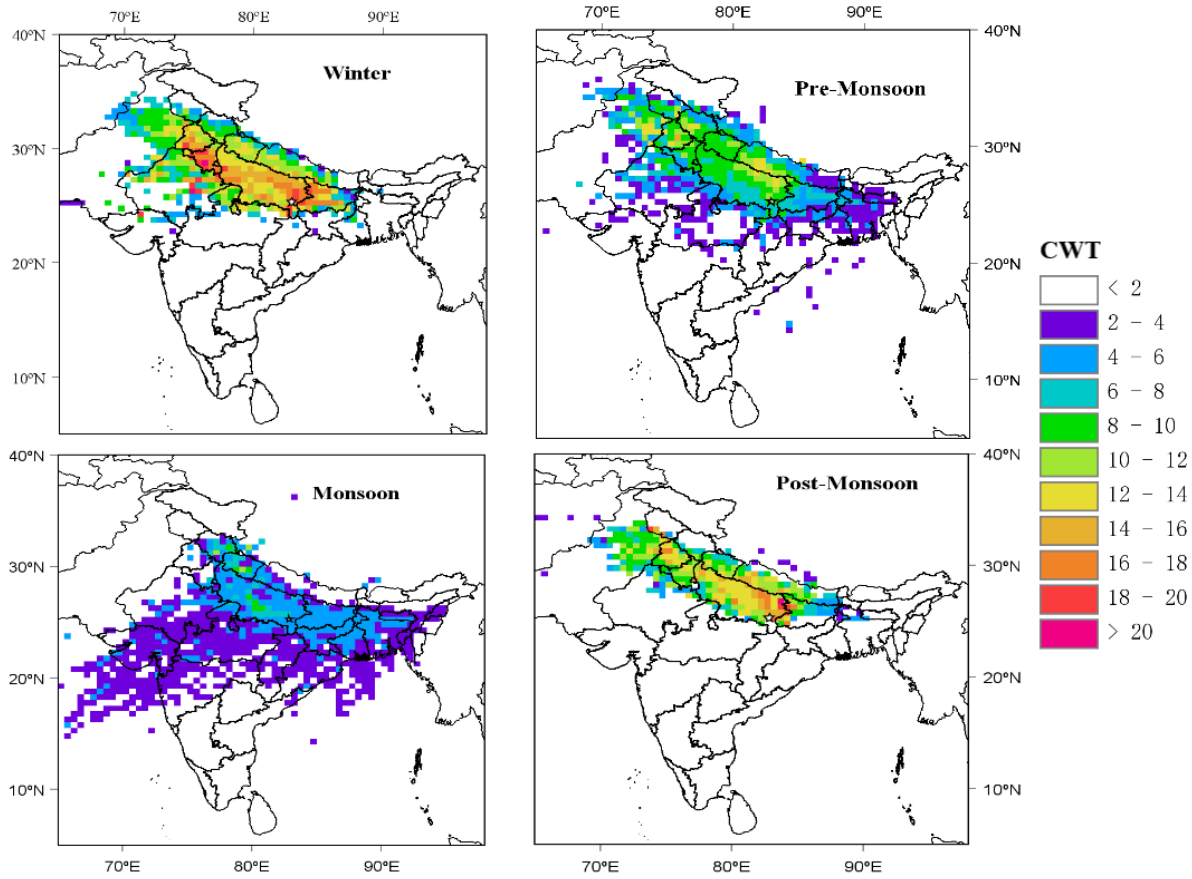

Figure 8. Weighted Concentration Weighted Trajectory (WCWT) maps of BC over Varanasi during 2009 to 2021

4.3 Radiative Impact of Black Carbon

In order to calculate BC aerosol radiative forcing, different BC optical properties are obtained from the OPAC model, following Verma et al. (2013). The single scattering albedo (SSA) and asymmetry parameter of BC at 0.5 µm obtained from the OPAC model were 0.22 and 0.35, respectively, which are found to be similar to the values are reported for the Brahmaputra River Valley region during 2013–14 (Tiwari et al., 2016b) and Kolkata during 2009–10 (Verma et al., 2013). The AOD caused due to BC (i.e., AOD_{BC}) shows strong seasonality and spectral dependency, as shown in Figure 9. AOD_{BC} is higher for the shorter wavelengths and gradually decreases with increasing wavelength. During pre-monsoon, AOD_{BC} shows the highest value and the highest standard deviation for all the wavelengths, compared to other seasons. The seasonal variation of AOD_{BC} at 0.5µm was highest during pre-monsoon season (0.178±0.102), followed

388 by winter (0.135±0.050), post-monsoon (0.129±0.069), and it was the least for the monsoon
389 season (0.068±0.031) due to possible wet scavenging.

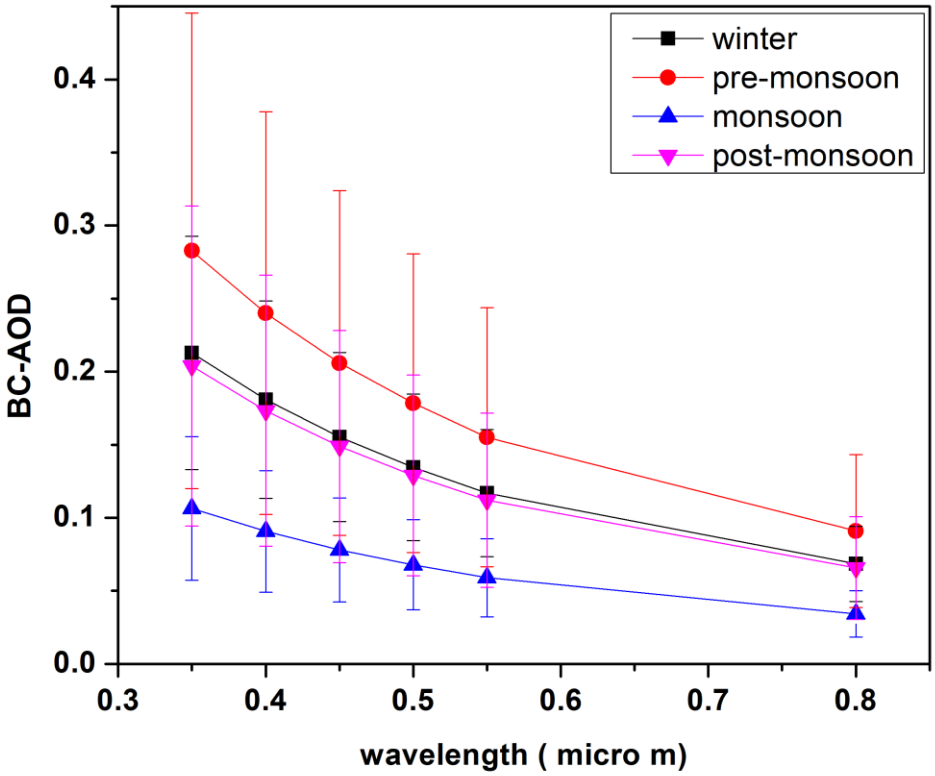

390

391 *Figure9. Seasonal variation of OPAC model derived BC-AOD during 2009 to 2021*

The SBDART model (Ricchiazzi et al., 1998) is used to compute shortwave (0.30–3.0 μm) direct BC aerosol radiative forcing ($DARF_{BC}$), separately for the top of the atmosphere (TOA) and surface (SUR).The estimated monthly BC aerosol radiative forcing is in the range of –7.0 to –125.3 W m^{-2} (mean: –30.1 ± 18.9 W m^{-2}) at the surface (ARF SUR) and +2.6 to +43.4 W m^{-2} (mean: 10.3 ± 6.4 W m^{-2}) at the top of the atmosphere (ARF TOA). However, the resultant BC radiative forcing in the atmosphere (ARF ATM) is found in the range of +9.7 to +168.7 W m^{-2} (mean: 40.5 ± 25.2 W m^{-2}). The negative BCARF-SUR value suggests a cooling effect at the surface, while a positive value of BC ARF-TOA over the study region shows a warming effect at the top of the atmosphere. The resultant atmospheric forcing is consequently positive, indicating a net warming effect throughout the study period. Interannual variation in BC-ARF is shown in Figure 10 (c), whereas, monthly mean variation in the BC-ARF is shown in Figure 10 (a). Similar to BC mass concentration trend shown in figure 2, an overall decreasing trend in BC atmospheric forcing (-1.94 W m^{-2} yr^{-1}) is also observed over the station, with a slight increasing trend till 2012 and decreasing trend thereafter.

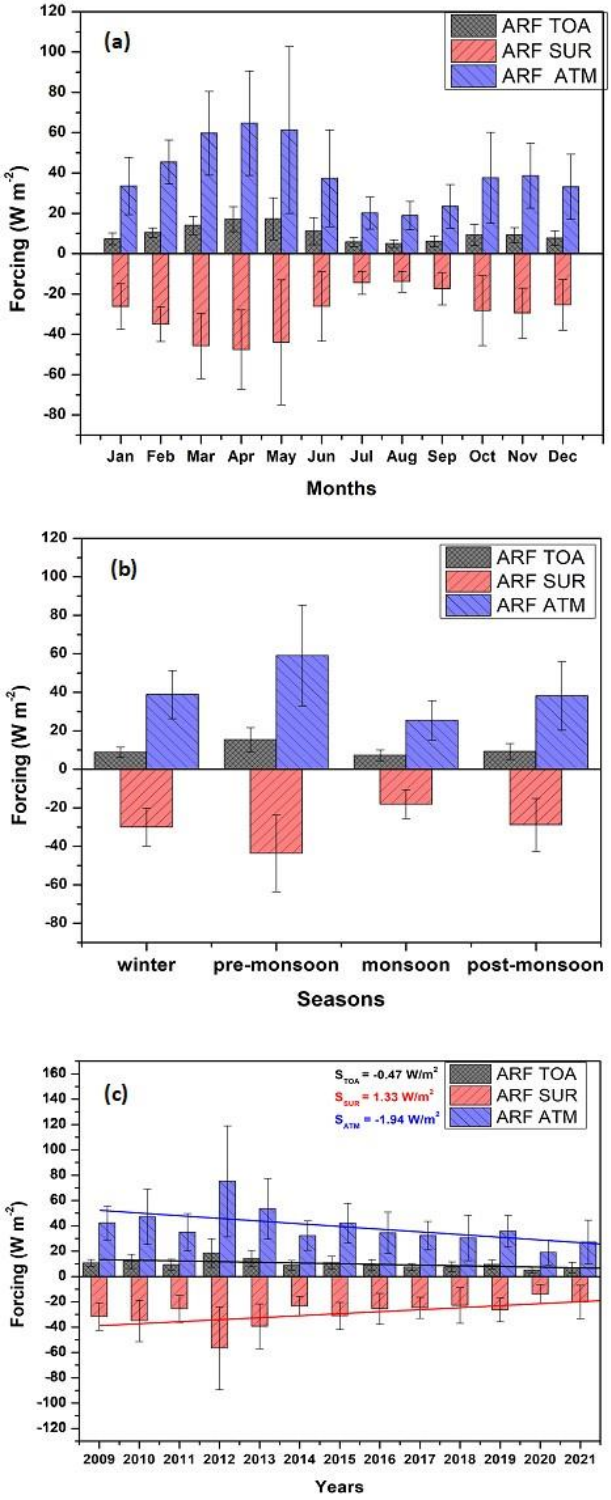

Figure 10. (a) Monthly variation in BC aerosol radiative forcing over Varanasi. (b) Seasonal variation of BC Aerosol Radiative forcing over Varanasi during 2009 – 2021. (c) Annual variation of BC Aerosol Radiative forcing over Varanasi during 2009 to 2021.

Lowest value of BC-ARF is during the monsoon months is caused due to less BC mass concentration over the region, whereas high values of BC-ARF are observed during the summer

months. Low BC concentration during 2020 reflects the prevailing COVID-19 situations and due to the governmental restrictions across the country that ultimately resulted in the lowest BC ARF-ATM during 2020. On the contrary, high BC concentration and BC ARF-ATM during 2012 is possibly due to less rainfall, accompanied with unusually high fire events in the IGP region, and favorable meteorological conditions. The seasonal variation of the BC ARF is shown in Figure 10 (b). Large variability in the BC radiative forcing is observed between different seasons at TOA, SUR, and ATM. Across all the seasons, the highest BC-ARF is observed during the pre-monsoon season at Varanasi despite of low BC concentration during pre-monsoon season, as compared to winter and post-monsoon seasons. The results indicate important role of boundary layer dynamics in modulating the surface mass concentration of pollutants, and hence the ARF. High boundary layer height (Figure 1) during the pre-monsoon season resulted in highest BC-AOD (Figure 9) and ultimately highest ARF for that season (Figure 10 (b)). Similar behavior in seasonal BC-ARF were found in a study for the Brahmaputra River Valley region over Guwahati during 2014 with the highest BC-ARF in the atmosphere during the pre-monsoon season, followed by the winter season than post-monsoon and monsoon season (Tiwari et al., 2016b). Maximum BC-ARF in the atmosphere was found during the winter season in a study over Dhanbad (28.0 W m^{-2}) during 2013 (Singh et al., 2018), over Hyderabad (33.5 Wm^{-2}) during 2009–2010 (Dumka et al., 2013), and over New Delhi (65.8 W m^{-2}) during 2010 (Surendran et al., 2013). Bhat et al., (2017) reported maximum BC-ARF values at TOA (5.8 W m^{-2}), SUR (-52.3 W m^{-2}), and ATM (58.2 W m^{-2}) during the post-monsoon period and minimum BC-ARFs values at TOA (2.3 W m^{-2}), SUR (-26.6 W m^{-2}), and ATM (28.0 W m^{-2}) during the pre-monsoon period over Srinagar during 2013. The average BC-ARFs values at TOA, SUR, and ATM were +9.5 W m^{-2}, −21.1 W m^{-2} and +30.6 W m^{-2}, +8.1, −20.8 W m^{-2}, and +28.0 W m^{-2}, for Guwahati during 2014 (Tiwari et al., 2016b) and Dhanbad during 2013 (Singh et al., 2018), respectively . The BC-ARF in the atmosphere over Hyderabad during 2009-2010 were reported to be 33.5 ± 7.0 W m^{-2} in winter, 31.8 ± 12.9 W m^{-2} in pre-monsoon, 18.9 ± 6.7 W m^{-2} in post-monsoon, and 13.2± 1.7 W m^{-2} in monsoon seasons (Dumka et al., 2013), which is less as compared to the values reported over Varanasi in the present study. Bisht et al. (2016) reported high values of BC ARF at TOA, SUR, and ATM over New Delhi during winter 2015. Seasonal mean BC-ARF values at TOA, SUR, and ATM over New Delhi were 20.9 ± 1.9 W m^{-2}, -75.5 ± 10.5 W m^{-2}, and 96.5 ± 12.3 W m^{-2} which was relatively higher than that the values reported over Varanasi during the same period.

The average BC-ARF over Varanasi at TOA, SUR, and ATM is 10.3 ± 6.4 W m^{-2}, -30.1± 18.9 W m^{-2}, and 40.5 ± 25.2 W m^{-2} during the entire study period indicates strong climatic impact of BC over the observation site. Modified Mann-Kendal and Sen's test show significant trend for the intra-annual and seasonal variability in BC-ARF at TOA, SUR, and ATM. Sen's slop estimator shows seasonal trend is maximum for post-monsoon and minimum for monsoon season (Figure 11). Inter-annual decreasing trend is observed for BC-ARF TOA and BC-ARF ATM while it showed increasing trend for BC-ARF SUR with slope value –0.47, – 1.94 and 1.33 W m^{-2} yr^{-1}, respectively, indicating that the heating effect due to BC is decreasing within the atmosphere and also that the cooling at the top of the atmosphere is decreasing over the region. The observed decreasing trend in BC-ARF ATM is found to be in association with the observed decreasing trend in BC mass concentration (as shown in Figure 2) over Varanasi, which indicates a slight reduction in the atmospheric warming due to BC aerosols. The average heating rate due to BC was 1.14±0.71 K day^{-1} with maximum heating observed during May 2012 (4.73 K day^{-1}) and minimum during August 2020 (0.27 K day^{-1})

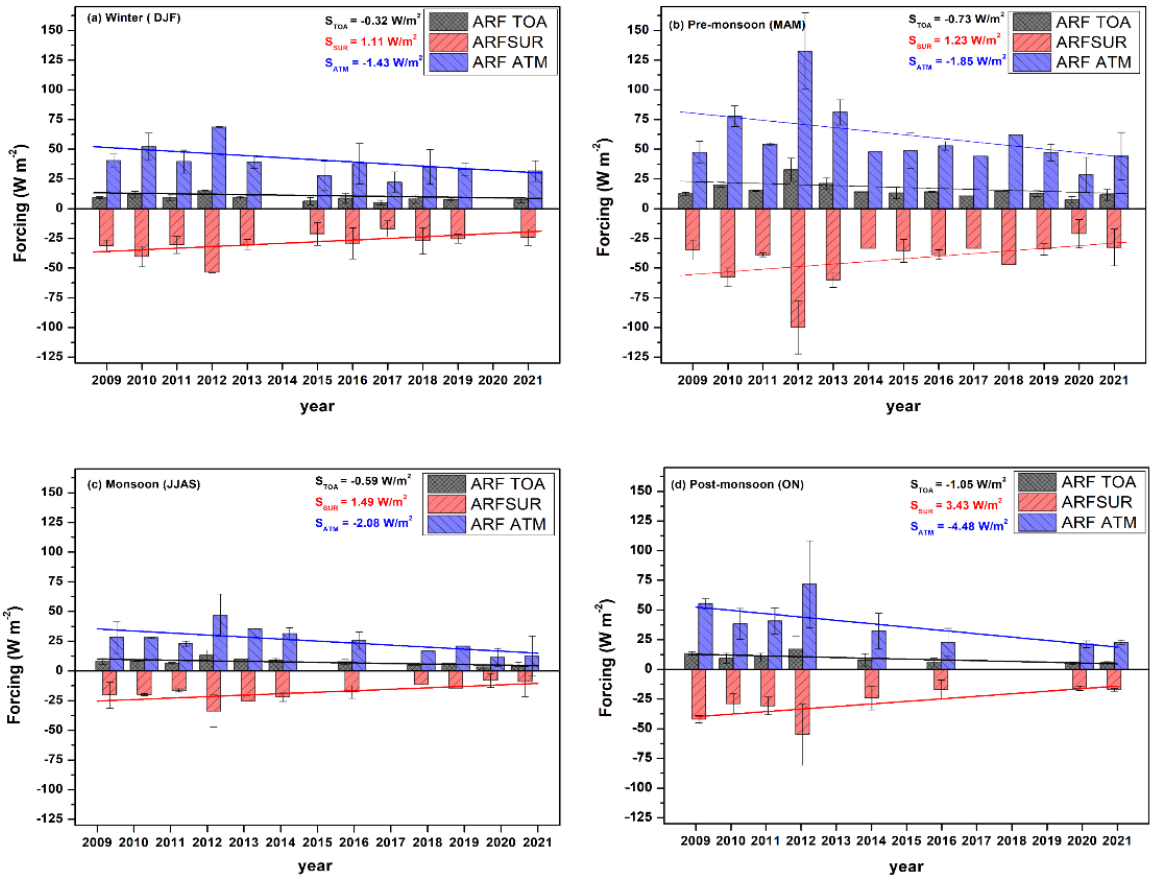

Figure11. Each year seasonal BC-ARF with in the atmosphere (W/m2) during 2009 to 2021 over Varanasi.

5. Conclusions

The long-term (13 years from 2009-2021) observation of surface BC mass concentration (mean: 9.25 ± 7.66 µg m−3) at a centrally located middle IGP station, Varanasi, a representative site in middle IGP, was used for the first time to investigate its diurnal and seasonal variability, long-term seasonal and annual trends, along with the associated BC optical and radiative implications. The main conclusions of the present study are listed below:

1. BC mass concentration shows a sharp diurnal pattern with two peaks in all the season across the study period, one peak in morning hours and other in late evening hours.

2. BC levels exhibited strong seasonal patterns, peaking during winter (14.67 ± 5.33 µg m^{-3}), followed by post-monsoon (12.60 ± 4.87 µg m^{-3}), while reaching a low during the monsoon (4.40 ± 1.70 µg m^{-3}). Winter period BC increase was driven by local factors like biomass burning, fossil fuel usage, and poor dispersion conditions. In contrast, BC during the pre-monsoon and post-monsoon periods was linked to crop residue burning in and around the regions. Monsoon rainfall effectively removed BC aerosols, causing its minimal levels during the monsoon season.

3. All the seasons show a significant decreasing trend in BC mass concentration over the study region, with the highest rate of decrease in post-monsoon (–1.86 µg $m^{-3}yr^{-1}$) and the least decrease during the pre-monsoon season (–0.31 µg $m^{-3}yr^{-1}$). On the annual basis, BC shows a decreasing trend of –0.47 µg $m^{-3}yr^{-1}$ over Varanasi during 2009 to 2021.

4. The AOD caused due to BC (AOD_{BC}) obtained from the OPAC model shows strong seasonality and spectral dependency. During pre-monsoon, AOD_{BC} shows the highest values for all the wavelengths, compared to other seasons. The seasonal variation of AOD_{BC} at 0.5µm was highest during pre-monsoon (0.178±0.1), followed by winter (0.135±0.05), post-monsoon seasons (0.129±0.07), and it was the least for the monsoon season (0.068±0.03) due to low BC concentrations from the possible wet scavenging process.

5. The variation of estimated monthly BC aerosol radiative forcing is in the range of –7.0 to –125.3 W m^{-2} (–30.1 ± 18.9 W m^{-2}) at the surface, +2.6 to +43.4 W m^{-2} (10.3 ± 6.4 W m^{-2}) at the top of the atmosphere, and +9.7 to +168.7 W m^{-2} (40.5 ± 25.2 W m^{-2}) in the atmosphere.

6. Across all the seasons, the highest BC-ARF is observed during the pre-monsoon (59±26.2 W m^{-2}) at Varanasi, despite of low BC concentration as compared to winter (38.9±12.5 W m^{-2}) and post-monsoon (38.1±17.9 W m^{-2}) seasons. The results indicate important role of boundary layer dynamics in modulating the ARF. High boundary layer height during the pre-monsoon season resulted in highest AOD_{BC} for the pre-monsoon and ultimately highest ARF during the season.

7. There is a significant trend for the intra-annual and seasonal variability in BC-ARF at TOA, SUR, and ATM. A decreasing trend in BC-ARF in the atmosphere (1.94 W m^{-2} yr^{-1}) is found to be associated with the observed decreasing trend in BC mass concentration, which indicates a slight reduction in the atmospheric warming due to BC aerosols.

Acknowledgments

The study is funded by the ISRO-ARFI. Authors BJM is thankful to ISRO-ARFI for the research fellowship, Authors MKS and RSS is thankful to ISRO-ARFI. Authors MKS and NM are thankful to BHU-IoE for the support. We acknowledge the Indian Metrological Department for the provision of the Metrological data, the NOAA Air resource Laboratory (ARL) for the provision of HYSPLIT model (https://www.ready.noaa.gov). The BC data used in the paper can be obtained from PI, ISRO-ARFI of ISRO-Geosphere Biosphere Programme (https://arfinet.vssc.gov.in/arfinet/index.html).

References

Ackerman, A.S., Toon, O.B., Stevens, D.E., Heymsfield, A.J., Ramanathan, V., Welton, E.J., 2000. Reduction of tropical cloudiness by soot. Science (80-.). 288, 1042–1047. https://doi.org/10.1126/science.288.5468.1042

Bhat, M.A., Romshoo, S.A., Beig, G., 2017. Aerosol black carbon at an urban site-Srinagar, Northwestern Himalaya, India: Seasonality, sources, meteorology and radiative forcing. Atmos. Environ. 165, 336–348. https://doi.org/10.1016/j.atmosenv.2017.07.004

514 Bisht, D.S., Tiwari, S., Dumka, U.C., Srivastava, A.K., Safai, P.D., Ghude, S.D., Chate, D.M.,
515 Rao, P.S.P., Ali, K., Prabhakaran, T., Panickar, A.S., Soni, V.K., Attri, S.D., Tunved, P.,
516 Chakrabarty, R.K., Hopke, P.K., 2016. Tethered balloon-born and ground-based
517 measurements of black carbon and particulate profiles within the lower troposphere during the
518 foggy period in Delhi, India. Sci. Total Environ. 573, 894–905.
519 https://doi.org/10.1016/j.scitotenv.2016.08.185

520 Bond, T.C., Bergstrom, R.W., 2006. Light absorption by carbonaceous particles: An
521 investigative review. Aerosol Sci. Technol. 40, 27–67.
522 https://doi.org/10.1080/02786820500421521

523 Bond, T.C., Doherty, S.J., Fahey, D.W., Forster, P.M., Berntsen, T., Deangelo, B.J., Flanner,
524 M.G., Ghan, S., Kärcher, B., Koch, D., Kinne, S., Kondo, Y., Quinn, P.K., Sarofim, M.C.,
525 Schultz, M.G., Schulz, M., Venkataraman, C., Zhang, H., Zhang, S., Bellouin, N., Guttikunda,
526 S.K., Hopke, P.K., Jacobson, M.Z., Kaiser, J.W., Klimont, Z., Lohmann, U., Schwarz, J.P.,
527 Shindell, D., Storelvmo, T., Warren, S.G., Zender, C.S., 2013. Bounding the role of black
528 carbon in the climate system: A scientific assessment. J. Geophys. Res. Atmos. 118, 5380–
529 5552. https://doi.org/10.1002/jgrd.50171

530 Census of India, 2011. District Census Handbook Varanasi Part XII-A 1–416.

531 CLARKE, A., NOONE, K., 1985. Soot in the arctic snowpack: a cause for perturbations in
532 radiative transfer. Atmos. Environ. 19, 2045–2053.
533 https://doi.org/10.1016/j.atmosenv.2007.10.059

534 Collaud Coen, M., Andrews, E., Alastuey, A., Arsov, T.P., Backman, J., Brem, B.T.,
535 Bukowiecki, N., Couret, C., Eleftheriadis, K., Flentje, H., Fiebig, M., Gysel-Beer, M., Hand,
536 J.L., Hoffer, A., Hooda, R., Hueglin, C., Joubert, W., Keywood, M., Kim, J.E., Kim, S.-W.,
537 Labuschagne, C., Lin, N.-H., Lin, Y., Lund Myhre, C., Luoma, K., Lyamani, H., Marinoni,
538 A., Mayol-Bracero, O.L., Mihalopoulos, N., Pandolfi, M., Prats, N., Prenni, A.J., Putaud, J.-
539 P., Ries, L., Reisen, F., Sellegri, K., Sharma, S., Sheridan, P., Sherman, J.P., Sun, J., Titos, G.,
540 Torres, E., Tuch, T., Weller, R., Wiedensohler, A., Zieger, P., Laj, P., 2020. Multidecadal
541 trend analysis of in situ aerosol radiative properties around the world. Atmos. Chem. Phys. 20,
542 8867–8908. https://doi.org/10.5194/acp-20-8867-2020

543 Conant, W.C., Nenes, A., Seinfeld, J.H., 2002. Black carbon radiative heating effects on cloud
544 microphysics and implications for the aerosol indirect effect. 1. Extended Köhler theory. J.
545 Geophys. Res. Atmos. 107, 1–9. https://doi.org/10.1029/2002JD002094

546 Ding, A.J., Huang, X., Nie, W., Sun, J.N., Kerminen, V.M., Petäjä, T., Su, H., Cheng, Y.F.,
547 Yang, X.Q., Wang, M.H., Chi, X.G., Wang, J.P., Virkkula, A., Guo, W.D., Yuan, J., Wang,
548 S.Y., Zhang, R.J., Wu, Y.F., Song, Y., Zhu, T., Zilitinkevich, S., Kulmala, M., Fu, C.B., 2016.
549 Enhanced haze pollution by black carbon in megacities in China. Geophys. Res. Lett. 43,
550 2873–2879. https://doi.org/10.1002/2016GL067745

551 Dumka, U.C., Kaskaoutis, D.G., Devara, P.C.S., Kumar, R., Kumar, S., Tiwari, S.,
552 Gerasopoulos, E., Mihalopoulos, N., 2019. Year-long variability of the fossil fuel and wood
553 burning black carbon components at a rural site in southern Delhi outskirts. Atmos. Res.
554 https://doi.org/10.1016/j.atmosres.2018.09.016

555 Dumka, U.C., Kaskaoutis, D.G., Tiwari, S., Safai, P.D., Attri, S.D., Soni, V.K., Singh, N.,
556 Mihalopoulos, N., 2018. Assessment of biomass burning and fossil fuel contribution to black

carbon concentrations in Delhi during winter. Atmos. Environ. 194, 93–109. https://doi.org/10.1016/j.atmosenv.2018.09.033

Dumka, U.C., Manchanda, R.K., Sinha, P.R., Sreenivasan, S., Moorthy, K.K., Suresh Babu, S., 2013. Temporal variability and radiative impact of black carbon aerosol over tropical urban station Hyderabad. J. Atmos. Solar-Terrestrial Phys. 105–106, 81–90. https://doi.org/10.1016/j.jastp.2013.08.003

Flanner, M.G., Zender, C.S., Hess, P.G., Mahowald, N.M., Painter, T.H., Ramanathan, V., Rasch, P.J., 2009. Springtime warming and reduced snow cover from carbonaceous particles. Atmos. Chem. Phys. 9, 2481–2497. https://doi.org/10.5194/acp-9-2481-2009

Flanner, M.G., Zender, C.S., Randerson, J.T., Rasch, P.J., 2007. Present-day climate forcing and response from black carbon in snow. J. Geophys. Res. Atmos. 112, 1–17. https://doi.org/10.1029/2006JD008003

Hansen, A.D.A., Rosen, H., Novakov, T., 1984. The aethalometer — An instrument for the real-time measurement of optical absorption by aerosol particles. Sci. Total Environ. 36, 191–196. https://doi.org/https://doi.org/10.1016/0048-9697(84)90265-1

Hansen, J., Nazarenko, L., 2004. Soot climate forcing via snow and ice albedos. Proc. Natl. Acad. Sci. 101, 423–428. https://doi.org/10.1073/pnas.2237157100

Haywood, J.M., Shine, K.P., 1995. The effect of anthropogenic sulfate and soot aerosol on the clear sky planetary radiation budget. Geophys. Res. Lett. 22, 603–606. https://doi.org/10.1029/95GL00075

Hess, M., Koepke, P., Schult, I., 1998. Optical Properties of Aerosols and Clouds: The Software Package OPAC. Bull. Am. Meteorol. Soc. 79, 831–844. https://doi.org/10.1175/1520-0477(1998)079<0831:OPOAAC>2.0.CO;2

Huang, K., Zhuang, G., Lin, Y., Wang, Q., Fu, J.S., Zhang, R., Li, J., Deng, C., Fu, Q., 2012. Impact of anthropogenic emission on air quality over a megacity - Revealed from an intensive atmospheric campaign during the Chinese Spring Festival. Atmos. Chem. Phys. 12, 11631–11645. https://doi.org/10.5194/acp-12-11631-2012

Jacobson, M.Z., 2001. Strong radiative heating due to the mixing state of black carbon in atmospheric aerosols. Nature 409, 695–697. https://doi.org/10.1038/35055518

Kalluri, R.O.R., Gugamsetty, B., Kotalo, R.G., Nagireddy, S.K.R., Tandule, C.R., Thotli, L.R., Shaik, N.H., Maraka, V.R., Rajuru, R.R., Surendran Nair, S.B., 2017. Seasonal variation of near surface black carbon and satellite derived vertical distribution of aerosols over a semi-arid station in India. Atmos. Res. 184, 77–87. https://doi.org/10.1016/j.atmosres.2016.09.003

Kanawade, V.P., Srivastava, A.K., Ram, K., Asmi, E., Vakkari, V., Soni, V.K., Varaprasad, V., Sarangi, C., 2020. What caused severe air pollution episode of November 2016 in New Delhi? Atmos. Environ. 222, 117125. https://doi.org/10.1016/j.atmosenv.2019.117125

Kang, S., Zhang, Y., Qian, Y., Wang, H., 2020. A review of black carbon in snow and ice and its impact on the cryosphere. Earth-Science Rev. 210, 103346. https://doi.org/10.1016/j.earscirev.2020.103346

Kant, Y., Shaik, D.S., Mitra, D., Chandola, H.C., Babu, S.S., Chauhan, P., 2020. Black carbon aerosol quantification over north-west Himalayas: Seasonal heterogeneity, source

apportionment and radiative forcing. Environ. Pollut. 257, 113446. https://doi.org/10.1016/j.envpol.2019.113446

Kedia, S., Ramachandran, S., Kumar, A., Sarin, M.M., 2010. Spatiotemporal gradients in aerosol radiative forcing and heating rate over Bay of Bengal and Arabian Sea derived on the basis of optical, physical, and chemical properties. J. Geophys. Res. Atmos. 115, 1–17. https://doi.org/10.1029/2009JD013136

Kendall, M.G., 1957. Rank Correlation Methods. Biometrika 44, 298. https://doi.org/10.2307/2333282

Koepke, P., Gasteiger, J., Hess, M., 2015. Technical Note: Optical properties of desert aerosol with non-spherical mineral particles: Data incorporated to OPAC. Atmos. Chem. Phys. 15, 5947–5956. https://doi.org/10.5194/acp-15-5947-2015

Kumar, S., Singh, A., Srivastava, A. K., Sahu, S. K., Hooda, R. K., Dumka, U. C., & Pathak, V. (2021). Long-term change in aerosol characteristics over Indo-Gangetic Basin: How significant is the impact of emerging anthropogenic activities? Urban Climate, 38, 100880.

Kumar, M., Raju, M.P., Singh, R.K., Singh, A.K., Singh, R.S., Banerjee, T., 2017. Wintertime characteristics of aerosols over middle Indo-Gangetic Plain: Vertical profile, transport and radiative forcing. Atmos. Res. 183, 268–282. https://doi.org/10.1016/j.atmosres.2016.09.012

Kumar, Manish, Raju, M.P., Singh, R.S., Banerjee, T., 2017. Impact of drought and normal monsoon scenarios on aerosol induced radiative forcing and atmospheric heating in Varanasi over middle Indo-Gangetic Plain. J. Aerosol Sci. 113, 95–107. https://doi.org/10.1016/j.jaerosci.2017.07.016

Latha, R., Murthy, B.S., Lipi, K., Srivastava, M.K., Kumar, M., 2017. Absorbing aerosols, possible implication to crop yield - a comparison between IGB stations. Aerosol Air Qual. Res. 17, 693–705. https://doi.org/10.4209/aaqr.2016.02.0054

Li, Z., Guo, J., Ding, A., Liao, H., Liu, J., Sun, Y., Wang, T., Xue, H., Zhang, H., Zhu, B., 2017. Aerosol and boundary-layer interactions and impact on air quality. Natl. Sci. Rev. 4, 810–833. https://doi.org/10.1093/nsr/nwx117

Lodhi, N.K., Beegum, S.N., Singh, S., Kumar, K., 2013. Aerosol climatology at Delhi in the western Indo-Gangetic Plain: Microphysics, long-term trends, and source strengths. J. Geophys. Res. Atmos. 118, 1361–1375. https://doi.org/10.1002/jgrd.50165

Manoj, M.R., Satheesh, S.K., Moorthy, K.K., Gogoi, M.M., Babu, S.S., 2019. Decreasing Trend in Black Carbon Aerosols Over the Indian Region. Geophys. Res. Lett. 46, 2903–2910. https://doi.org/10.1029/2018GL081666

Mann, H.B., 1945. Nonparametric Tests Against Trend. Econometrica 13, 245. https://doi.org/10.2307/1907187

Meehl, G.A., Arblaster, J.M., Collins, W.D., 2008. Effects of black carbon aerosols on the Indian monsoon. J. Clim. 21, 2869–2882. https://doi.org/10.1175/2007JCLI1777.1

Mohammad, L., Mondal, I., Bandyopadhyay, J., Pham, Q.B., Nguyen, X.C., Dinh, C.D., Al-Quraishi, A.M.F., 2022. Assessment of spatio-temporal trends of satellite-based aerosol optical depth using Mann–Kendall test and Sen's slope estimator model. Geomatics, Nat. Hazards Risk 13, 1270–1298. https://doi.org/10.1080/19475705.2022.2070552

Murari, V., Kumar, M., Singh, N., Singh, R.S., Banerjee, T., 2016. Particulate morphology and elemental characteristics: variability at middle Indo-Gangetic Plain. J. Atmos. Chem. 73, 165–179. https://doi.org/10.1007/s10874-015-9321-5

Murari, V., Singh, N., Ranjan, R., Singh, R.S., Banerjee, T., 2020. Source apportionment and health risk assessment of airborne particulates over central Indo-Gangetic Plain. Chemosphere 257, 127145. https://doi.org/10.1016/j.chemosphere.2020.127145

Nenes, A., Conant, W.C., Seinfeld, J.H., 2002. Black carbon radiative heating effects on cloud microphysics and implications for the aerosol indirect effect 2. Cloud microphysics. J. Geophys. Res. Atmos. 107, AAC 24-1-AAC 24-11. https://doi.org/10.1029/2002jd002101

Rajput, P., Sarin, M., Kundu, S.S., 2013. Atmospheric particulate matter (PM2.5), EC, OC, WSOC and PAHs from NE-Himalaya: Abundances and chemical characteristics. Atmos. Pollut. Res. 4, 214–221. https://doi.org/10.5094/APR.2013.022

Rajput, P., Sarin, M., Sharma, D., Singh, D., 2014. Characteristics and emission budget of carbonaceous species from post-harvest agricultural-waste burning in source region of the Indo-Gangetic plain. Tellus, Ser. B Chem. Phys. Meteorol. 66, 1–11. https://doi.org/10.3402/tellusb.v66.21026

Raju, M.P., Safai, P.D., Sonbawne, S.M., Naidu, C. V., 2015. Black carbon radiative forcing over the Indian Arctic station, Himadri during the Arctic Summer of 2012. Atmos. Res. 157, 29–36. https://doi.org/10.1016/j.atmosres.2015.01.013

Ricchiazzi, P., Yang, S., Gautier, C., Sowle, D., 1998. SBDART: A Research and Teaching Software Tool for Plane-Parallel Radiative Transfer in the Earth's Atmosphere. Bull. Am. Meteorol. Soc. 79, 2101–2114. https://doi.org/10.1175/1520-0477(1998)079<2101:SARATS>2.0.CO;2

Sandeep, P., Saradhi, I. V., Pandit, G.G., 2013. Seasonal variation of black carbon in fine particulate matter (PM 2.5) at the tropical coastal city of Mumbai, India. Bull. Environ. Contam. Toxicol. 91, 605–610. https://doi.org/10.1007/s00128-013-1108-2

Sen, A., Abdelmaksoud, A.S., Nazeer Ahammed, Y., Alghamdi, M.., Banerjee, T., Bhat, M.A., Chatterjee, A., Choudhuri, A.K., Das, T., Dhir, A., Dhyani, P.P., Gadi, R., Ghosh, S., Kumar, K., Khan, A.H., Khoder, M., Maharaj Kumari, K., Kuniyal, J.C., Kumar, M., Lakhani, A., Mahapatra, P.S., Naja, M., Pal, D., Pal, S., Rafiq, M., Romshoo, S.A., Rashid, I., Saikia, P., Shenoy, D.M., Sridhar, V., Verma, N., Vyas, B.M., Saxena, M., Sharma, A., Sharma, S.K., Mandal, T.K., 2017. Variations in particulate matter over Indo-Gangetic Plains and Indo-Himalayan Range during four field campaigns in winter monsoon and summer monsoon: Role of pollution pathways. Atmos. Environ. 154, 200–224. https://doi.org/10.1016/j.atmosenv.2016.12.054

Singh, A., Srivastava, A. K., Pathak, V., & Shukla, A. K. (2022). Quantifying the impact of biomass burning and dust storm activities on aerosol characteristics over the Indo-Gangetic Basin. Atmospheric Environment, 270, 118893.

Singh, A., Srivastava, A. K., Varaprasad, V., Kumar, S., Pathak, V., Shukla, A. K., 2021. Assessment of near-surface air pollutants at an urban station over the central Indo-Gangetic Basin: Role of pollution transport pathways. Meteorol. Atmos. Phys. 133, 1127–1142.

Singh, B.P., Srivastava, A.K., Tiwari, S., Singh, S., Singh, R.K., Bisht, D.S., Lal, D.M., Singh, A.K., Mall, R.K., Srivastava, M.K., 2014. Radiative impact of fireworks at a tropical Indian location: A case study. Adv. Meteorol. 2014. https://doi.org/10.1155/2014/197072

Singh, B.P., Tiwari, S., Hopke, P.K., Singh, R.S., Bisht, D.S., Srivastava, A.K., Singh, R.K., Dumka, U.C., Singh, A.K., Rai, B.N., Srivastava, M.K., 2015. Seasonal inhomogeneity of soot particles over the central indo-gangetic plains, India: Influence of meteorology. J. Meteorol. Res. 29, 935–949. https://doi.org/10.1007/s13351-015-5041-7

Singh, R.P., Kumar, S., Singh, A.K., 2018. Elevated black carbon concentrations and atmospheric pollution around singrauli coal-fired thermal power plants (India) using ground and satellite data. Int. J. Environ. Res. Public Health 15. https://doi.org/10.3390/ijerph15112472

Singh, S., Tiwari, S., Gond, D.P., Dumka, U.C., Bisht, D.S., Tiwari, Shani, Pandithurai, G., Sinha, A., 2015. Intra-seasonal variability of black carbon aerosols over a coal field area at Dhanbad, India. Atmos. Res. 161–162, 25–35. https://doi.org/10.1016/j.atmosres.2015.03.015

Singh, S., Tiwari, S., Hopke, P.K., Zhou, C., Turner, J.R., Panicker, A.S., Singh, P.K., 2018. Ambient black carbon particulate matter in the coal region of Dhanbad, India. Sci. Total Environ. 615, 955–963. https://doi.org/10.1016/j.scitotenv.2017.09.307

Soni, P., Tripathi, S.N., Srivastava, R., 2018. Radiative effects of black carbon aerosols on Indian monsoon: a study using WRF-Chem model. Theor. Appl. Climatol. 132, 115–134. https://doi.org/10.1007/s00704-017-2057-1

Srivastava, A. K., Ram, K., Pant, P., Hegde, P., Joshi, H., 2012. Black carbon aerosols over central Himalayas: Implications to climate forcing. Environmental Research Letters, 7, 014002, doi:10.1088/1748-9326/7/1/014002.

Srivastava, A.K., Mehrotra, B.J., Singh, A., Singh, V., Bisht, D.S., Tiwari, S., Srivastava, M.K., 2020. Implications of different aerosol species to direct radiative forcing and atmospheric heating rate. Atmos. Environ. 241, 117820. https://doi.org/10.1016/j.atmosenv.2020.117820

Stein, A.F., Draxler, R.R., Rolph, G.D., Stunder, B.J.B., Cohen, M.D., Ngan, F., 2015. Noaa's hysplit atmospheric transport and dispersion modeling system. Bull. Am. Meteorol. Soc. 96, 2059–2077. https://doi.org/10.1175/BAMS-D-14-00110.1

Surendran, D.E., Beig, G., Ghude, S.D., Panicker, A.S., Manoj, M.G., Chate, D.M., Ali, K., 2013. Radiative forcing of black carbon over Delhi. Int. J. Photoenergy 2013. https://doi.org/10.1155/2013/313652

Talukdar, S., Venkat Ratnam, M., Ravikiran, V., Chakraborty, R., 2019. Influence of Black Carbon Aerosol on the Atmospheric Instability. J. Geophys. Res. Atmos. 124, 5539–5554. https://doi.org/10.1029/2018JD029611

Tiwari, S., Dumka, U.C., Kaskaoutis, D.G., Ram, K., Panicker, A.S., Srivastava, M.K., Tiwari, Shani, Attri, S.D., Soni, V.K., Pandey, A.K., 2016a. Aerosol chemical characterization and role of carbonaceous aerosol on radiative effect over Varanasi in central Indo-Gangetic Plain. Atmos. Environ. 125, 437–449. https://doi.org/10.1016/j.atmosenv.2015.07.031

Tiwari, S., Kumar, R., Tunved, P., Singh, S., Panicker, A.S., 2016b. Significant cooling effect on the surface due to soot particles over Brahmaputra River Valley region, India: An impact on

721 regional climate. Sci. Total Environ. 562, 504–516.
722 https://doi.org/10.1016/j.scitotenv.2016.03.157

723 Tiwari, S., Srivastava, A.K., Bisht, D.S., Bano, T., Singh, S., Behura, S., Srivastava, M.K.,
724 Chate, D.M., Padmanabhamurty, B., 2009. Black carbon and chemical characteristics of
725 PM10 and PM 2.5 at an urban site of North India. J. Atmos. Chem. 62, 193–209.
726 https://doi.org/10.1007/s10874-010-9148-z

727 Tiwari, S., Srivastava, A.K., Singh, A.K., Singh, S., 2015. Identification of aerosol types over
728 Indo-Gangetic Basin: implications to optical properties and associated radiative forcing.
729 Environ. Sci. Pollut. Res. 22, 12246–12260. https://doi.org/10.1007/s11356-015-4495-6

730 Verma, S., Ghosh, S., Boucher, O., Wang, R., Menut, L., 2022. Black carbon health impacts in
731 the Indo-Gangetic plain: Exposures, risks, and mitigation. Sci. Adv. 8, 1–12.
732 https://doi.org/10.1126/sciadv.abo4093

733 Verma, S., Pani, S.K., Bhanja, S.N., 2013. Sources and radiative effects of wintertime black
734 carbon aerosols in an urban atmosphere in east India. Chemosphere 90, 260–269.
735 https://doi.org/10.1016/j.chemosphere.2012.06.063

736 Virkkula, A., Mäkelä, T., Hillamo, R., Yli-Tuomi, T., Hirsikko, A., Hämeri, K., Koponen, I.K.,
737 2007. A simple procedure for correcting loading effects of aethalometer data. J. Air Waste
738 Manag. Assoc. 57, 1214–1222. https://doi.org/10.3155/1047-3289.57.10.1214

739 Wang, Y.Q., 2019. An Open Source Software Suite for Multi-Dimensional Meteorological Data
740 Computation and Visualisation. J. Open Res. Softw. 7, 1–9. https://doi.org/10.5334/jors.267

741 Wang, Y.Q., 2014. MeteoInfo: GIS software for meteorological data visualization and analysis.
742 Meteorol. Appl. 21, 360–368. https://doi.org/10.1002/met.1345

743 Weingartner, E., Saathoff, H., Schnaiter, M., Streit, N., Bitnar, B., Baltensperger, U., 2003.
744 Absorption of light by soot particles: Determination of the absorption coefficient by means of
745 aethalometers. J. Aerosol Sci. 34, 1445–1463. https://doi.org/10.1016/S0021-8502(03)00359-
746 8

747 Yue, S., Wang, C.Y., 2004. Water Tower of the Yellow River in a Changing Climate: Toward an
748 integrated assessment. Water Resour. Manag. 18, 201–218.

749 Zhao, B., Jiang, J.H., Gu, Y., Diner, D., Worden, J., Liou, K.-N., Su, H., Xing, J., Garay, M.,
750 Huang, L., 2017. Decadal-scale trends in regional aerosol particle properties and their linkage
751 to emission changes. Environ. Res. Lett. 12, 054021. https://doi.org/10.1088/1748-
752 9326/aa6cb2

753 Zhu, C.-S., Qu, Y., Huang, H., Chen, J., Dai, W.-T., Huang, R.-J., & Cao, J.-J. (2021). Black
754 carbon and secondary brown carbon, the dominant light absorption and direct radiative
755 forcing contributors of the atmospheric aerosols over the Tibetan Plateau. Geophysical
756 Research Letters, 48, e2021GL092524. https://doi.org/10.1029/2021GL092524

757

758